# Metal-Transfer-Micromolded Three-Dimensional Microelectrode Arrays for *in-vitro* Brain-Slice Recordings

Swaminathan Rajaraman, Seong-O Choi, Maxine A. McClain, *Member, IEEE*, James D. Ross, *Student Member, IEEE*, Michelle C. LaPlaca, and Mark G. Allen, *Fellow, IEEE*

***Abstract*—We report the development of metal-transfer-micromolded 3-D microelectrode arrays (3-D MEAs) and demonstrate successful electrical characterization, biocompatibility measurements, and electrophysiological recordings from rat hippocampal brain slices with these MEAs. Metal transfer micromolding is introduced as a manufacturing technology for producing nonplanar metallized patterned microelectromechanical-systems devices such as MEAs on polymeric substrates. This technology provides a self-aligned metallization scheme that eliminates the need for complex 3-D lithography. Two techniques, i.e., an intentionally formed nonplanar mold and a shadow mask, are demonstrated for the self-aligned metallization scheme. The MEAs have further been packaged using custom-designed commercial printed circuit boards and insulated using parylene deposition. Recording sites have been defined using two techniques: laser micromachining/reactive ion etching (RIE) of parylene and selective deposition of parylene using a "capping" technique. Electrical (impedance spectroscopy), biocompatibility (2-D planar cultures of neurons), electrophysiological (tissue slice recordings) characterizations of the MEAs are successfully demonstrated in this paper. The impedance of the electrodes was modeled based on a classical equivalent circuit, and high-frequency impedance estimation techniques were studied. We believe this fabrication approach offers an attractive route to disposable and biocompatible 3-D MEAs, utilizable by the neurophysiology and pharmacology communities. [2010-0254]**

***Index Terms*—Electrophysiological spike recordings, metal transfer micromolding (MTM), neuronal interfacing, three-dimensional microelectrode arrays (3-D MEAs).**

## I. Introduction

MICROELECTRODE arrays (MEAs) are important tools to study single neurons and the functional organization of neural networks and tissues. Dissociated cultures of neurons are becoming more popular in many physiological studies due to their superior performance compared with *in vivo* models in terms of electrical recording and stimulation, pharmacological manipulation, and imaging [1]. Due to the size of the cells involved which is on the microscale, an attractive technique for manufacturing MEAs is microfabrication, which has been used to make planar (2-D) devices. Several microfabricated 2-D arrays have been reported in the last 35 years for extracellular stimulation [2] and recordings [3] from cultured neuronal cells and brain slices. These have traditionally been fabricated on common microfabrication substrates, such as glass and silicon [4], [5]. Recently, however, there has been a shift from traditional substrates to nontraditional ones like polyimide [6] and polydimethylsiloxane (PDMS) [7] as these materials provide the potential for cost-effective large-volume micromanufacturing. Furthermore, the ability to produce MEAs with these materials provides familiarity to the end users: the biologists who prefer to work with familiar materials like polymers. Two-dimensional MEAs are limited in their applicability to 3-D cell constructs (like tissue slices or 3-D dissociated cultures) mainly due to attenuation of the electrical signal from cells [leading to poor signal-to-noise ratios (SNRs)] as the neuron–microelectrode distance increases. In the case of tissue slices, the dead cell layers (which occur due to the dissection procedure) serve as the source for poor SNRs. Heuschkel *et al.* [8] report that protruding electrodes achieve higher signal amplitudes in spike recordings due to the better penetration of the slice and the ability to get past the dead cell layers. The electrodes reported by Heuschkel *et al.* are less than 100 $\mu$m above the planar surface. Thus, a technology that combines 3-D functionality (higher than 100 $\mu$m), scalability, and mass manufacturability is required to address the current and future needs of the *in vitro* electrophysiological, neurophysiological, and pharmacological communities. This, however, is challenging as lithography on nonplanar surfaces is not easily accomplished. Approaches that have been reported for

Manuscript received September 10, 2010; revised December 14, 2010; accepted December 15, 2010. Date of publication February 4, 2011; date of current version April 1, 2011. This work was supported in part by the U.S. National Institute of Health Bioengineering Research Partnerships under Grant EB00786-01. Subject Editor C. Liu.

S. Rajaraman and M. A. McClain were with the School of Electrical and Computer Engineering, Georgia Institute of Technology, Atlanta, GA 30332 USA. They are now with Axion BioSystems, Inc., Atlanta, GA 30332 USA (e-mail: srajaraman@axionbio.com; mcclain@axion-biosystems.com).

S.-O. Choi was with the School of Electrical and Computer Engineering, Georgia Institute of Technology, Atlanta, GA 30332 USA. He is now with the School of Chemical and Biomolecular Engineering, Georgia Institute of Technology, Atlanta, GA 30332 USA (e-mail: seongo.choi@gmail.com).

J. D. Ross was with The Wallace H. Coulter Department of Biomedical Engineering, Georgia Tech/Emory University, Atlanta, GA 30332 USA. He is now with Axion BioSystems, Inc., Atlanta, GA 30332 USA (e-mail: jross@axionbio.com).

M. C. LaPlaca is with The Wallace H. Coulter Department of Biomedical Engineering, Georgia Tech/Emory University, Atlanta, GA 30332 USA (e-mail: michelle.laplaca@bme.gatech.edu).

M. G. Allen is with the School of Electrical and Computer Engineering, Georgia Institute of Technology, Atlanta, GA 30332 USA (e-mail: mallen@gatech.edu).

Color versions of one or more of the figures in this paper are available online at http://ieeexplore.ieee.org.

Digital Object Identifier 10.1109/JMEMS.2011.2105253

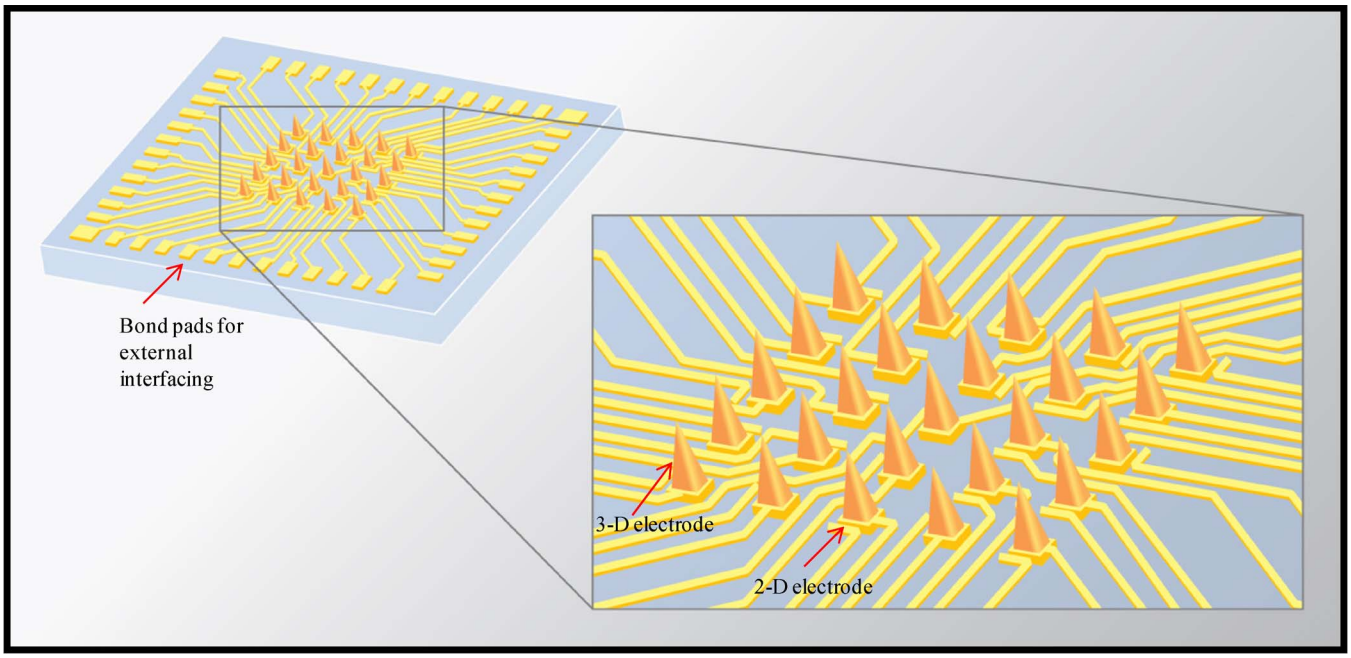


Fig. 1. Schematic of the proposed metal-transfer-micromolded 3-D MEA. The inset on the right shows the electrode area with 25 metallized towers (3-D electrodes) and 25 electrode traces (2-D electrodes).

nonplanar lithography include optimized resist coatings [9], laser micromachining [10], and electrodeposited resists [11]. In this paper, we report microfabrication and packaging technologies that we believe provide attractive alternative routes to address the needs listed earlier.

Microassembly is the most common approach in the microelectromechanical-systems (MEMS) community to fabricate *in vivo* 3-D MEAs. Approaches have been reported by Wise [12] to fabricate *in vivo* MEAs which are integrated with electronics for wireless data transmission. These probes are fabricated on silicon substrates using planar micromachining technologies and are optionally assembled to achieve a true 3-D form [13]. Recently, Rowe *et al.* [14] reported a microassembly of a series of microfabricated planar SU-8 towers to achieve 3-D MEAs for *in vitro* studies. Other 3-D MEA fabrication technologies reported include a combination of acid etching/sawing [15] and electrical discharge machining of a singular slab of metal like stainless steel or titanium [16]. The first integrated (and, hence, batch fabricated) fabrication approach toward protruding or spiked MEAs was reported by Thiebaud *et al.* [17] and Metz *et al.* [18]. These MEAs are manufactured in silicon and glass, respectively, but the reported heights of the electrodes are less than 100 $\mu$m. Takei *et al.* [19] recently reported an interesting approach for achieving 3-D MEAs integrated with electronics on the same chip based on vapor–liquid–solid growth of silicon probes to achieve the electrode structure. However, the height of the probes demonstrated in this paper was around 30 $\mu$m.

Approaches that lend themselves easily to mass manufacturing and/or large-area processing are attractive alternatives to microassembly or other types of processes for this application. Toward such a goal, micromolding and batch fabrication are reported in this paper toward the microfabrication of 3-D MEAs. Metal transfer micromolding (MTM) is introduced in this paper as a potential candidate for achieving 3-D MEAs with electrode heights of 300–500 $\mu$m or greater. The height of the electrodes can be controlled to suit the intended application. MTM has two distinct advantages which can be exploited to overcome the previously listed fabrication/production challenges: 1) a self-aligned metallization scheme that allows for simultaneous metallization/patterning of electrode towers at different heights and 2) a micromolding-based approach which lends itself to scaling and mass production. Fig. 1 shows the schematic of such a device, with the closer inset depicting the electrode area. The design chosen for the 3-D MEA is a 5 $\times$ 5 array of metallized towers in the center of the chip and electrodes at the bottom of each tower (2-D counterparts). All the electrodes can be individually addressed electrically at the periphery of the chip. The overall chip dimensions are 10 mm $\times$ 10 mm, with the towers themselves being 280 $\mu$m at the base with a pitch of 800 $\mu$m. The fabrication and packaging of such a device is reported in this paper. Detailed electrical characterization of these MEAs has been carried out with development of the background impedance theory from classical electrode–electrolyte interactions. This theory predicts that the real part of the impedance of microelectrodes at the higher frequencies (greater than 1 kHz) is related only to the base area of the electrodes which was explored experimentally. A scheme to fine-tune the impedance of a microelectrode to suit the application was developed. Furthermore, the impedance model demonstrated expected results for impedance variation with electrode size. The biocompatibility of the materials involved in constructing these MEAs has been evaluated with a 2-D planar culture of neurons. These MEAs have been further evaluated for their ability to record electrophysiological signals from hippocampal brain slices of postnatal rat pups.

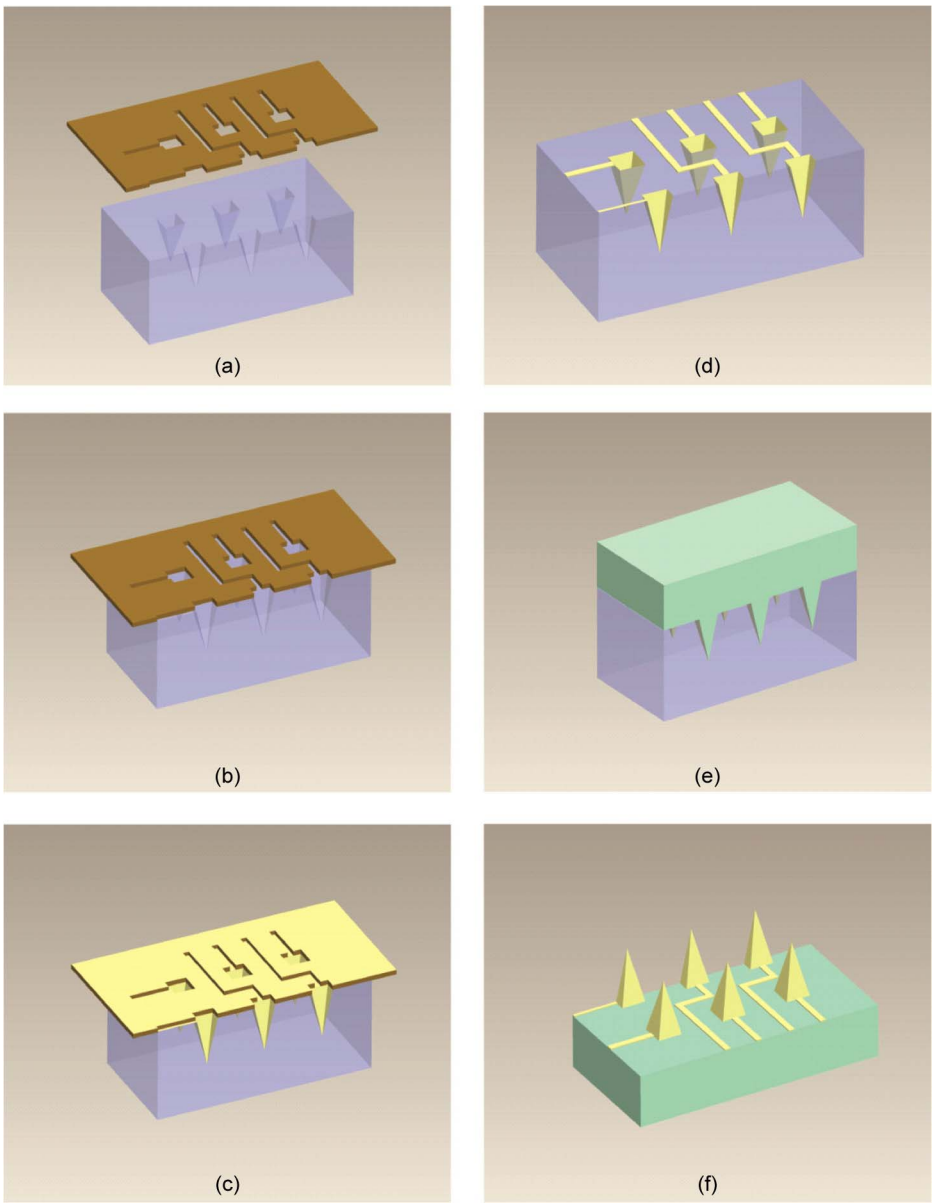


Fig. 2. Process flow for the shadow mask approach: (a) Separate fabrication of the PDMS mold and the Kapton shadow mask. (b) Alignment of the mask to the mold. (c) Deposition of a layer of gold (Au) and chromium (Cr) using a physical vapor deposition system. (d) Removal of the shadow mask. (e) Solvent-casting of the target polymer. (f) Demolding of the MTM 3-D MEA with metallized electrodes and metal traces.

## II. Microfabrication

### A. MTM: Shadow Mask Approach

The negative-tone epoxy SU-8 (*Micro-Chem, Inc.*, Newton, MA) has been used as a structural material in MEMS fabrication for sometime now [14], [20], [21]. Standard top-side and bottom-side exposures and inclined rotational exposures are utilized to define various shapes in SU-8 [22]. By utilizing micromolding, this rigid mold can be converted to a flexible mold fabricated using PDMS.

An important step toward the realization of manufacturing-friendly approaches for producing 3-D MEAs is self-aligned metallization and metal patterning. Three-dimensional fabrication to pattern metal in trenches or towers is a complex problem in MEMS and requires the difficult approaches listed in Section I. In order to simplify fabrication, we have developed an MTM-based approach [23] which can be thought of as an extension of 2-D metal transfer processes like those used in nanoimprinting [24]. This process exploits the surface energy difference between PDMS (19.8 mJ/cm$^2$ [25]) and other polymers (surface energy typically higher than PDMS) to transfer metal patterns from one to the other during the process of micromolding. This is shown in

$$W_{\text{sub-metal}} - W_{\text{PDMS-metal}} = (\gamma_{\text{sub}} - \gamma_{\text{PDMS}}) - (\gamma_{\text{sub-metal}} - \gamma_{\text{PDMS-metal}}) \quad (1)$$

where $W_{\text{sub-metal}}$ and $W_{\text{PDMS-metal}}$ are work functions of adhesion between polymeric substrate/metal and PDMS/metal, respectively. $\gamma_{\text{sub}}$ and $\gamma_{\text{PDMS}}$ represent surface energies of polymeric substrate and PDMS, respectively. $\gamma_{\text{sub-metal}}$ and $\gamma_{\text{PDMS-metal}}$ represent interfacial energies between substrate

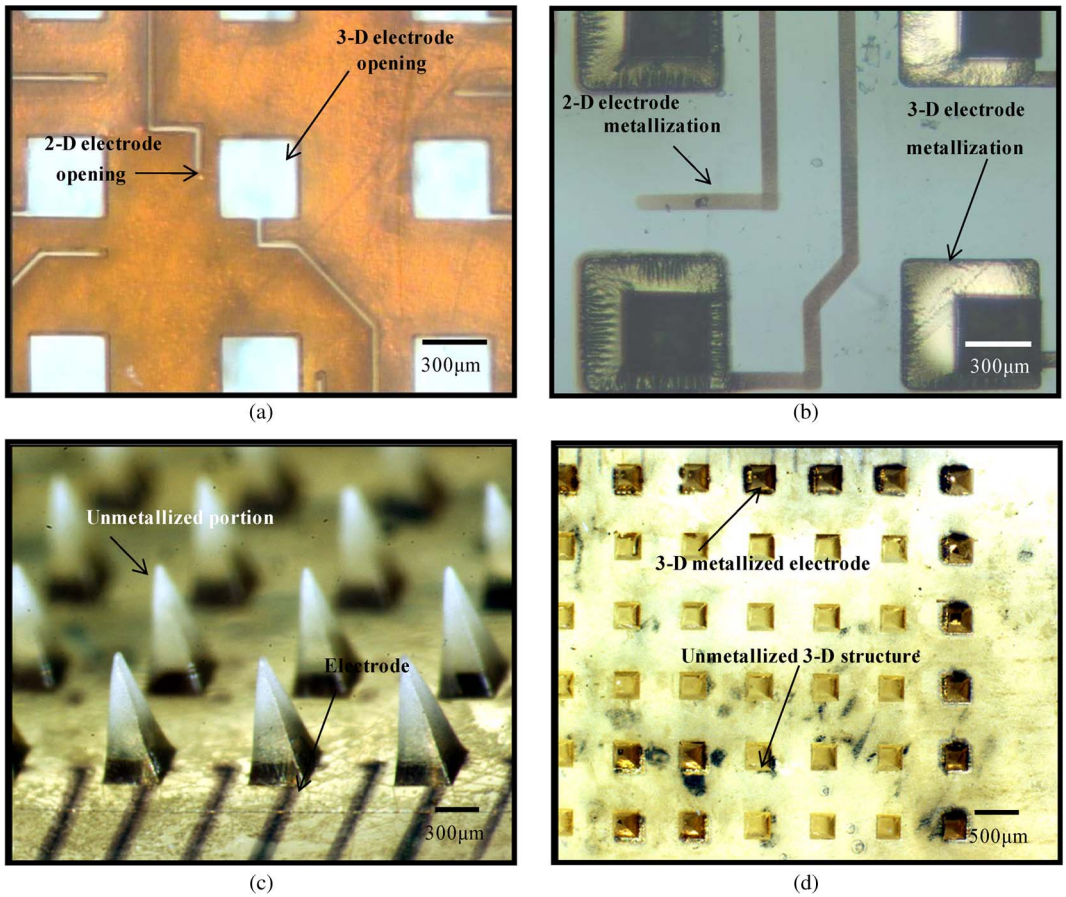


Fig. 3. Optical micrographs of (a) a laser micromachined Kapton shadow mask, (b) a PDMS mold selectively metallized using the shadow mask, (c) the side view of a demolded 3-D MEA (fabricated using SU-8) (metal traces (electrodes) are running along the height of the tower), and (d) the side view of a selectively metallized 3-D MEA.

and metal and between PDMS and metal, respectively. We have successfully demonstrated metal transfer during micromolding onto the following polymers: SU-8, polymethyl methacrylate (PMMA), and polyurethane (PU). Two separate approaches have been demonstrated to accomplish the metal transfer: 1) selective metal removal using an intentionally formed nonplanar mold using 2-D metal transfer, which is described in detail in the next section, and 2) selective metal deposition onto and into the mold features using a shadow mask. The shadow mask process is detailed in Fig. 2(a)–(f). It begins with the fabrication of a shadow mask [Fig. 2(a)] using an excimer laser (*Resonetics, Inc.*, Nashua, NH) ablation process of thin Kapton ($\sim$125 $\mu$m) sheets. The ablation is achieved at 250-mJ energy (20% attenuation) at the rate of 50–60 $\mu$m per cut. Feature sizes as small as 20 $\mu$m can be achieved using this recipe. This mask is then aligned with a PDMS mold [fabricated with inclined UV lithography and micromolding as described in [22], Fig. 2(b)] and held in place with pins. Alignment marks are micromachined on the shadow mask to aid this process (alignment accuracy of $\sim$25 $\mu$m; alignment is performed under a stereoscope and two pins secure the arrangement, and a shadow mask can be reused after etching the metal layers). A layer of Au/Cr (500 nm/10 nm) is evaporated [Fig. 2(c)] onto this mold using a filament evaporator (*Kurt J. Lesker Company*, Clairton, PA). The shadow mask is then removed [Fig. 2(d)], and the target polymer (PMMA, SU-8, or PU) is cast onto the mold [Fig. 2(d)]. The polymer is postprocessed and demolded from the PDMS mold [Fig. 2(e)]. Metal is transferred during this process from the PDMS to the target polymer. Fig. 3(a) and (b) shows optical micrographs of a Kapton shadow mask and the PDMS mold with metal deposited using the shadow mask. Fig. 3(c) and (d) shows optical images of a demolded SU-8 3-D MEA fabricated using this technique. However, this method suffers from a few disadvantages: 1) The process of making a shadow mask is time consuming and serial, 2) alignment of the shadow mask to the mold is nontrivial, and 3) due to coefficient-of-thermal-expansion mismatch between the mold (PDMS, 310 ppm/°C [26]) and the shadow mask (Kapton, 20 ppm/°C [27]), the resulting metal trace width is larger than the intended value, which could lead to potential shorting in high-density arrays. Hence, a nonplanar mold approach, which allows for self-alignment and eliminate these potential problems, was investigated. This technique is described in detail in the following section.

### *B. MTM: Nonplanar Mold Approach*

The microfabrication process using a nonplanar mold for a 3-D MEA is schematically shown in Fig. 4. It begins with the exposure of pyramidal pits on 700-$\mu$m-thick SU-8 [Fig. 4(a)] using inclined UV lithography. A second layer of SU-8 (100 $\mu$m thick) is spin coated on the mold without developing the first

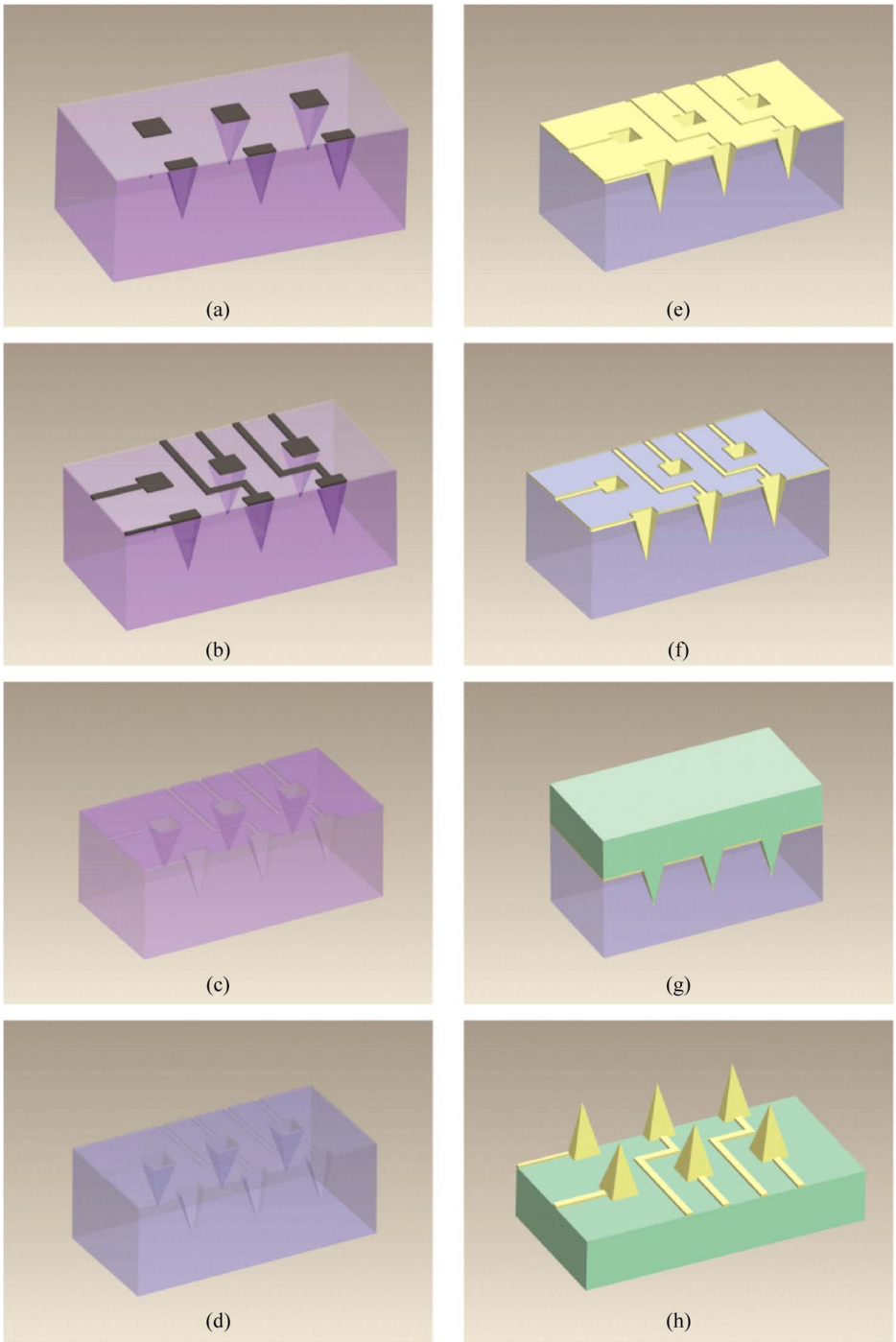


Fig. 4. Process flow for the nonplanar mold approach: (a) Inclined UV exposure of 700-$\mu$m-thick SU-8 to form trenches. (b) Top-side alignment of a second layer of SU-8 to form metal traces. (c) Development of both layers together to fabricate an SU-8 rigid master. (d) Fabrication of a flexible mold using micromolding. (e) Metallization of the mold using a physical vapor deposition tool. (f) Patterning of the electrodes using a high-surface-energy plate. (g) Solvent-casting of the target polymer. (h) Demolding of the 3-D MEA.

layer. A second mask that has the metal interconnection patterns is aligned with the first layer and then exposed [Fig. 4(b)]. Both layers are simultaneously developed after postexposure baking [Fig. 4(c)] to obtain a two-layer SU-8 rigid mold. A master structure is fabricated by casting premixed PDMS into this rigid mold. A sputtered Cr/Au (10 nm/150 nm) layer is used to aid the release of the master from the rigid mold. This master structure is metallized (using the same release layer), PDMS-cast, and cured to get a flexible PDMS mold. This nonplanar mold has the same patterns as the original rigid two-layer SU-8 mold [Fig. 4(d)]. To define the electrodes, an Au/Cr layer (500 nm/10 nm) is evaporated [Fig. 4(e)] on the flexible PDMS mold using a filament evaporator. Metal transfer is achieved by bringing a high-surface-energy plate (such as a silicon wafer or scotch tape) in contact with the metallized PDMS mold [Fig. 4(f)]. The metal is patterned at this step. This is accomplished by two mechanisms: 1) the fact that the surface energy of PDMS is lower than the plate that is in contact with

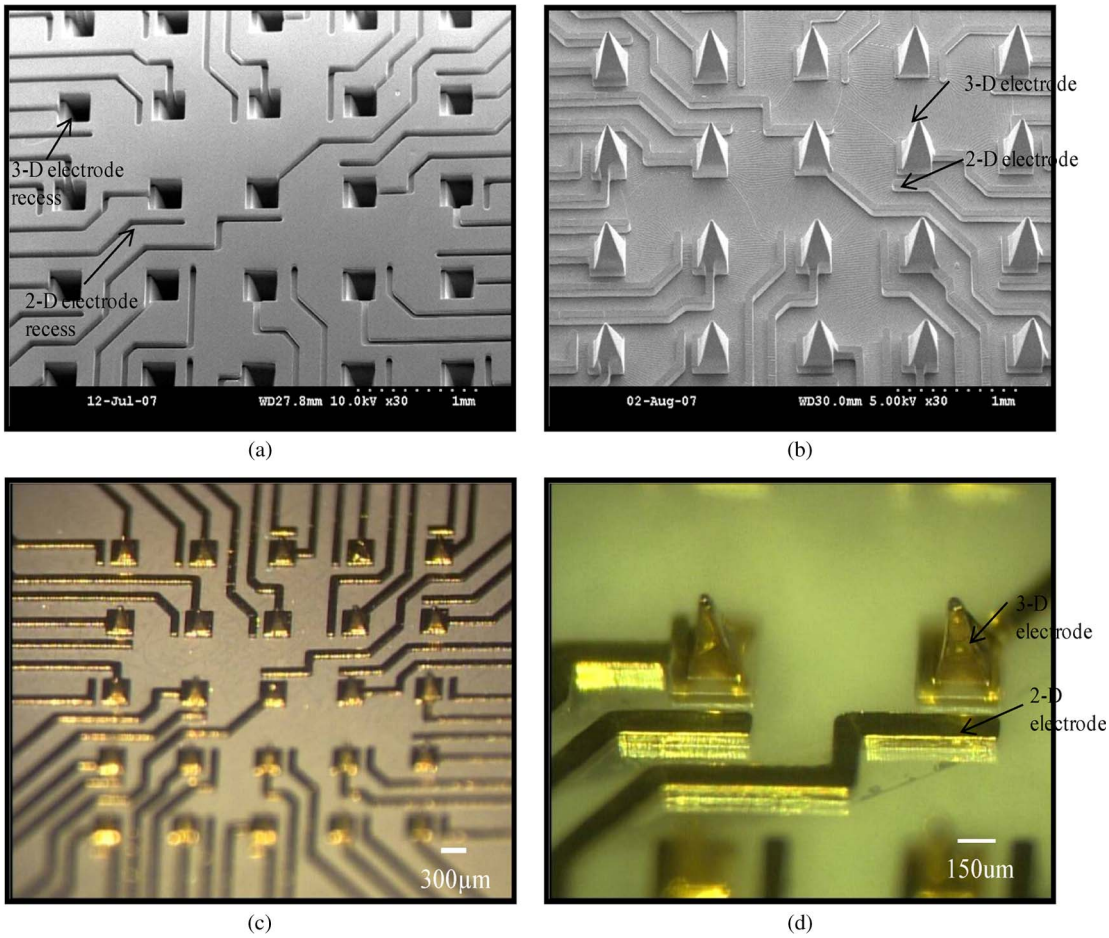


Fig. 5. SEMs and optical micrographs of (a) two-layer rigid SU-8 mold, (b) a flexible PDMS master fabricated from the SU-8 mold, (c) the side view of a demolded PMMA 3-D MEA [electrodes are provided both as metal traces (2-D) and metallized towers (3-D)], and (d) side view of a demolded PU 3-D MEA showing the clear distinction between 2-D and 3-D electrodes.

the mold and 2) the nonplanarity of the mold. Both of these enable geometrical isolation of the electrode patterns. Once the metal has been patterned, the target polymer can be cast onto and into the patterned PDMS mold [Fig. 4(g)]. Devices using several target polymers, including SU-8, PMMA, and PU, have been fabricated. Exposure (in the case of SU-8) with 5000 mJ of I-line UV and solvent casting (in the case of PMMA and PU) serves as a means of releasing/demolding the 3-D MEA from the PDMS mold [Fig. 4(h)]. This process yields a patterned 3-D MEA device that has 50 individually addressed 2-D and 3-D electrodes. Fig. 5(a) shows a SEM image of a two-layer rigid SU-8 mold. Fig. 5(b) shows a SEM image of the PDMS master fabricated from the SU-8 mold. Fig. 5(c) and (d) shows optical micrographs of the side views of a PMMA and a PU MEA, respectively. Electrodes are embedded in both the base layer and at the tips of the pyramids (300–500 $\mu$m above the planar surface), offering two levels of electrodes in the $z$-plane.

## III. Packaging

### A. 3-D MEA Packaging

The fabricated tower arrays need to be packaged for a complete 3-D MEA. Packaging is a nontrivial issue as microspaced electrodes need to be connected to macrospaced pads for electronics interfacing. Packaging accounts for over 70% of the cost of the final device in semiconductors, MEMS, and biomedical devices [28]. Hence, it is highly desirable that cost-effective solutions for packaging are in place as MEMS devices are being conceived and constructed. Several techniques have been developed to package these devices. The first technique is similar to the methods used in [10], but instead of wirebonding to connect the MEA to the bond pads of the packaging chip (fabricated from fused silica wafers using lift-off techniques), conductive epoxy (*Master Bond*, Hackensack, NJ) was utilized. In order to develop a manufacturing-friendly approach, commercial printed circuit boards (PCBs) were designed and fabricated. The design and layout for the PCBs was performed using CAD Soft Eagle (*CadSoft Computer Inc.*, Pembroke Pines, FL) and fabricated using a standard two-metal-layer (with a layer of FR4 in between the metal layers at *Custom PCB*, Kuala Lumpur, Malaysia) process. The top metal layer contains large macrosized pads for interfacing with external electronics (e.g., preamplifier). The bottom metal traces (connected to the top pads through plated vias) were terminated using bond pads (microsized) to attach to the 3-D MEA. The overall dimension of the PCB was designed to be 49 mm $\times$ 49 mm to be compatible with a Multichannel Systems (*Multichannel Systems*

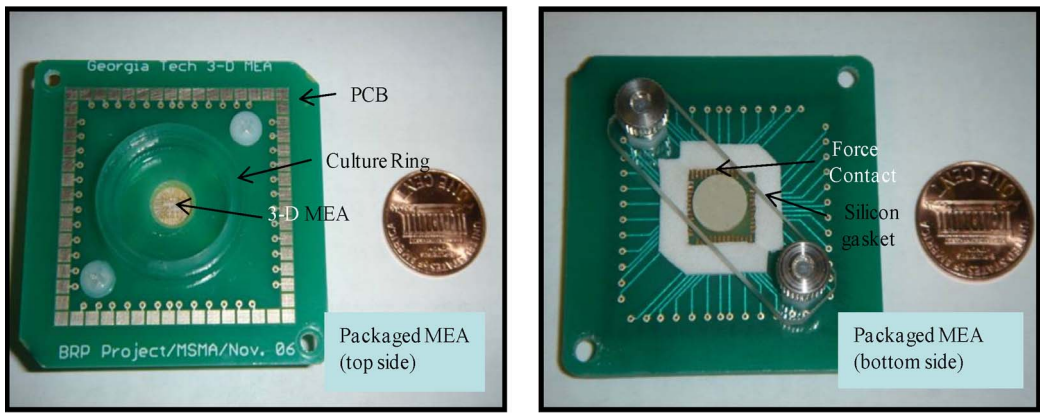


Fig. 6. (a) Optical photograph of a packaged 3-D MEA with the top side shown. We can clearly see the MEA, the culture ring, and the PCB macropads for electronics interfacing. (b) Optical photograph of a packaged 3-D MEA with the bottom side shown. A silicon gasket is used for alignment, and force contact is provided with an acrylic spacer for attaching the PCB to the MEA die.

*(MCS)*, Reutlingen, Germany) preamplifier setup which was used for the electrical and electrophysiological measurements (described in Section IV). A central port (dimensions: 12 mm) was also drilled as part of the PCB fabrication process to serve as an interface between the electrodes and tissue slices. It also serves as an optical port for microscopic imaging during experimentation. A process combining a self-alignment scheme (custom-made silicon gaskets attached to the back of the PCB onto which the MEA chips were placed) and force contact using an acrylic spacer (which held the MEA chip and PCB together in intimate contact) was developed to achieve packaging of the MTM 3-D MEA. This technique ensures that the assembly is simple and scales well to higher electrode counts.

Fig. 6(a) and (b) shows images of the packaged and assembled 3-D MEA. A culture ring (dimensions: OD—24 mm, ID—22 mm) was fabricated by laser micromachining ($CO_2$ laser, *New Hermes-Gravograph*, Duluth, GA) of acrylic sheets (thickness of 6 mm) and attached to the PCB using PDMS to complete the packaging. The culture ring serves two purposes: 1) acts as a containment ring for biological material and 2) holds the platinum electroplating (described in the following section) solution.

### B. Recording Site Electroplating

Commercial 2-D MEAs typically have a 5-$\mu$m layer of biocompatible insulation (SU-8) spin coated and recording sites defined for electrical stimulation and recording by planar lithography [29]. For the 3-D MEAs described in this paper, this is not possible due to the fact that the electrodes are 300–500 $\mu$m above the planar surface. Thus, nonconventional techniques have to be developed to passivate the MEAs and define the recording sites. Two techniques were evaluated in this paper—a process combining laser micromachining and reactive ion etching (RIE) of a conformally deposited polymer and selective deposition of this very same conformal polymer using a "capping process." Parylene has been selected as the conformally deposited polymer in this process. It is biocompatible [30] and can be deposited at relatively low temperatures compatible with polymer processing. Furthermore, it is laser micromachinable, as previously reported [10], [32]. FR4, the commonly used epoxy composite in PCBs, is a known cytotoxic substance [31]. To effectively insulate the substrate, a thin layer of PDMS was coated in the area surrounding the central port of the PCB (could come in contact with cells). A layer of parylene (5 $\mu$m thick to be compatible with commercial devices) was deposited over the entire packaged assembly (Parylene Deposition System, *Speciality Coating Systems*, Indianapolis, IN). The selective excimer laser micromachining of parylene deposited on thin metal has been described in detail in our previous work [10], [32]. These techniques were used to selectively ablate parylene. Recording sites (50 $\mu$m in size) were ablated on both 2-D and 3-D electrodes. The residual parylene from the laser microablation was effectively removed using a RIE ($CHF_3/O_2$ Plasma) process. This etch step targeted the removal of 1 $\mu$m of parylene. Impedance spectroscopy (described in the next section) was performed after this step, and the results are shown in Fig. 11(a). A selective deposition of parylene was additionally developed to simplify the insulation definition. A "3-D capping microdevice" was fabricated using SU-8, as described in techniques reported in our earlier publication [10]. These devices [Fig. 7(b)] were then utilized to selectively "cap" the 2-D and 3-D recording sites, as shown in Fig. 7(a), and subsequently, parylene was deposited on the entire structure. This process ensured simplification of the parylene definition and improved yields [Fig. 11(b)]. Platinum black was then electroplated onto the recording sites. Electroplating platinum black increases the surface area of the electrodes, serves to reduce the impedance, and ensures that high-frequency microelectrode characterization can be performed [33]. Ross [34] describes the design and implementation of a platinum electroplating setup in more detail. Platinum black is electroplated onto the recording sites of the 3-D MEA using a current density of 4.9 $\mu$A/cm$^2$ at room temperature using a solution of 1% chloroplatinic acid with 0.0025% HCl and 0.01% lead acetate (all diluted in DI water). Optical micrographs of electroplated recording sites are shown in Fig. 8.

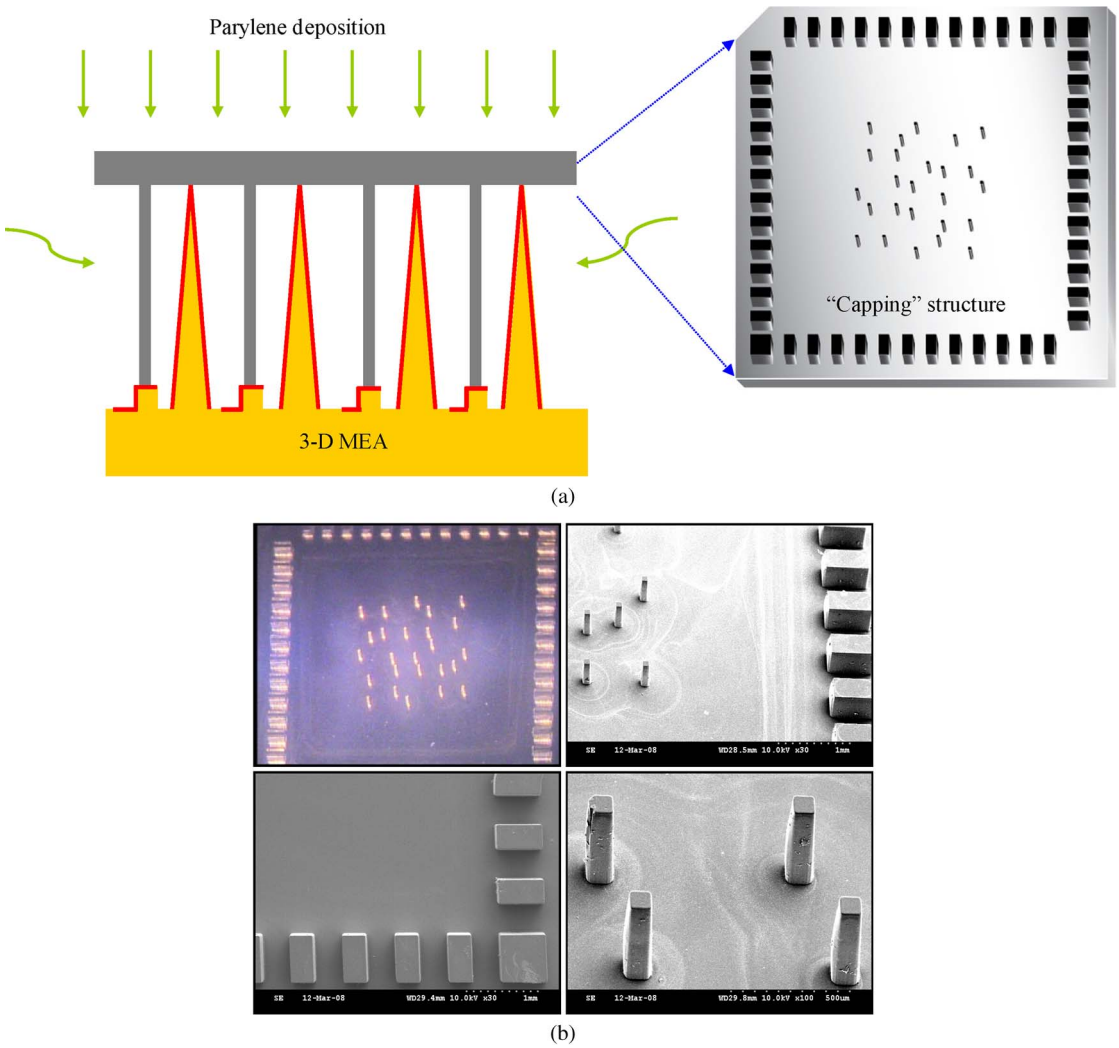


Fig. 7. "Capping technique" for deposition of parylene insulation: (a) Schematic of the capping technique. (b) Optical and SEM micrographs of the fabricated "capping" structures. These structures are microfabricated utilizing a double-sided exposure of SU-8 technique [10].

## IV. Testing and Results

### A. 3-D MEA Impedance Modeling

Material and physical properties of the electrode have profound influence on the stimulation and recording from neural tissue. Thus, explicit shaping of the impedance spectrum of a microelectrode depends on understanding how physical properties of the electrode (material, cross-sectional area, etc.) relate to this spectrum. Over the past decade, the microelectrode–electrolyte theory has been extensively studied [33]–[35], and we are not attempting to recreate the theory in this paper but this established theory has been applied to the MTM 3-D MEA to evaluate how experimental considerations relate to theoretical analysis. Remarkably, the complex electrode–electrolyte interface is described by a rather simple lumped-circuit model, shown in Fig. 9(a), consisting of an interface capacitance $C_I$ shunted by a charge-transfer resistance $R_T$ with a spreading resistance $R_S$. Each of these circuit elements is uniquely described by the electrochemical processes and electrode geometry [35]. This lumped-circuit model tuned to describe various 3-D electrode sizes (electrodes approximated to be circular with respect to a distant ground electrode) demonstrates the expected reduction in impedance with increase in size of the electrode, as shown in Fig. 9(b). This model provides a validation for the experimental data that are obtained (Fig. 11). Each of the components that make up this interface is related to either the surface-area/material properties of the electrodes ($C_I$ and $R_T$) or the base geometric area of the electrode ($R_S$)[35]. This has been demonstrated in the model by sensitivity analysis (increasing each of these parameters sequentially by 100 times while keeping the other two constant for a 50-$\mu$m-diameter circular electrode) and the impedance changes correspondingly, as shown in Fig. 10(a), with $R_T$ affecting the low-frequency spectrum, $C_I$ affecting the midband, and $R_S$ affecting the high-frequency band, respectively. Various parameters were extracted from the measured impedance data and compared with the data reported in the literature (and used in our impedance model), as shown in Table I. The extracted parameters agree in the same degree with model parameters as other MEA approaches where complex microfabrication is involved [18], [29], [33].

Of particular interest among these various parameters is the impedance in the higher frequency spectrum (1 kHz and above). This impedance is very important for electrophysiologists as

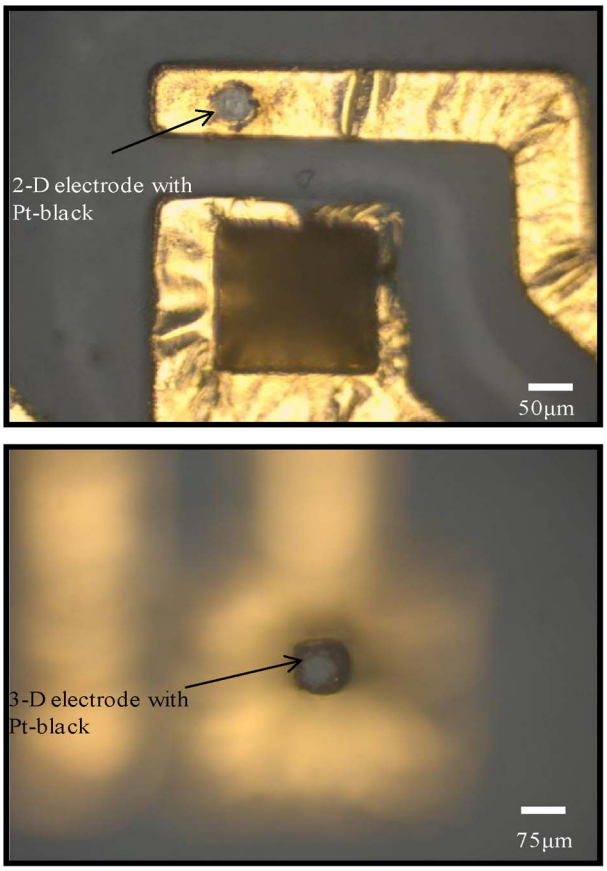


Fig. 8. Optical micrographs of the electroplated platinum black onto the MTM MEA recording sites. (Top) Pt on a 2-D recording site. (Bottom) Pt on a 3-D recording site.

the baseline noise is directly proportional to this impedance, as predicted by theory [33]. The interesting feature of this impedance is that it is directly related to the geometric area of the electrode and, hence, can be studied optically by measuring the electrode size. Thus, having a level of control over this process ensures that lower impedances can be accomplished at these frequencies. Since this high-frequency impedance is directly related to the base area of the electrode, it can potentially provide feedback to processing. For circular electrodes, this impedance is given by [32]

$$Rs = \frac{\rho}{4r} = \frac{\rho\sqrt{\Pi}}{4\,\mathrm{A}} \tag{2}$$

where $\rho$ is the resistivity of the medium, $r$ is the radius of the microelectrode, and $A$ is the base area of the electrode.

The geometric base area of the electrodes was measured under the microscope, and the impedance was plotted as a function of base area both based on theoretical predictions and experimental determination (at 10 kHz). This plot is shown in Fig. 10(b). Although a general trend (inverse variation as predicted) can be observed, there is significant variation in the results. The reasons for this can be traced back to the difficulty in measurement and control of the size of the electrodes with our current processes. This result is consistent with what was observed by other researchers in this area [33]. Furthermore, there is no accurate way to estimate the geometric base area of

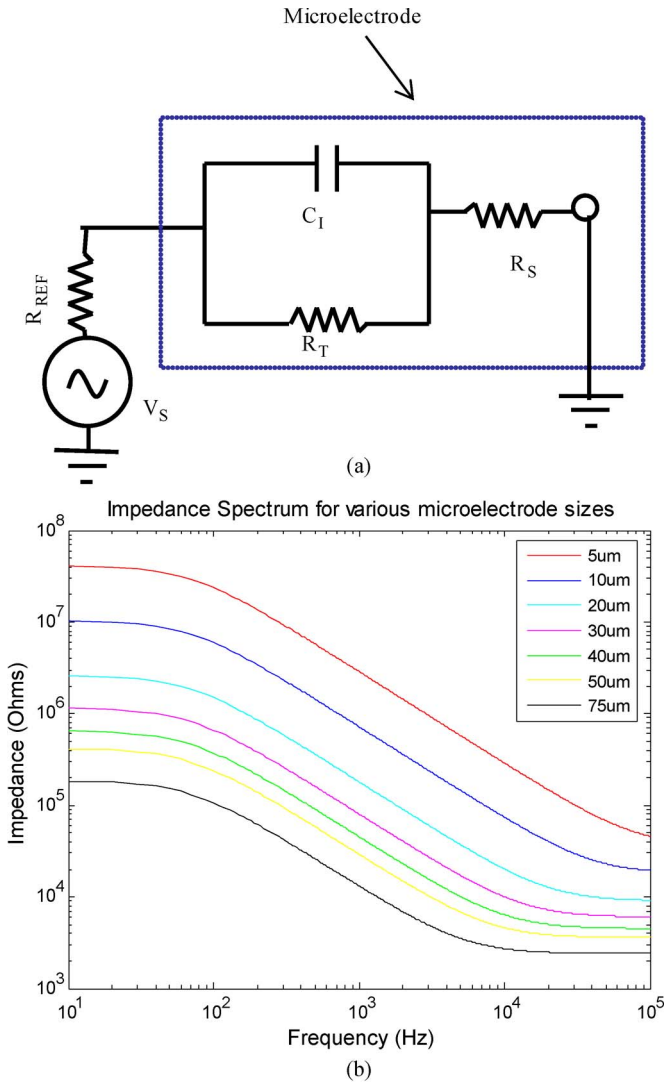


Fig. 9. Microelectrode impedance model. (a) Classic microelectrode–electrolyte circuit representation. (b) MATLAB modeling results for such a classic microelectrode of various sizes.

3-D electrodes which are shaped as cones rather than circles, thus exacerbating the problem (even though the assumption of circular electrodes was made, it was with the recognition that the modeling section was not the focus of this paper). Nevertheless, this technique, in combination with platinum deposition, provides a potential mechanism by which the high-frequency impedance of the electrode can be tuned to suit the application.

### B. 3-D MEA Impedance Spectrum Measurement

The electrical impedance spectroscopy of the fabricated 3-D MEA device may be used to evaluate the electrical properties of individual electrodes and can provide feedback to processing, as described previously. An example of this is platinum black not adhering well to the recording sites due to redeposition of parylene during laser micromachining. Therefore, it is critical to establish the viability of each electrode before biological testing. This is accomplished with a Stanford Research SR785 (*Stanford Research Systems*, Sunnyvale, CA) two-channel

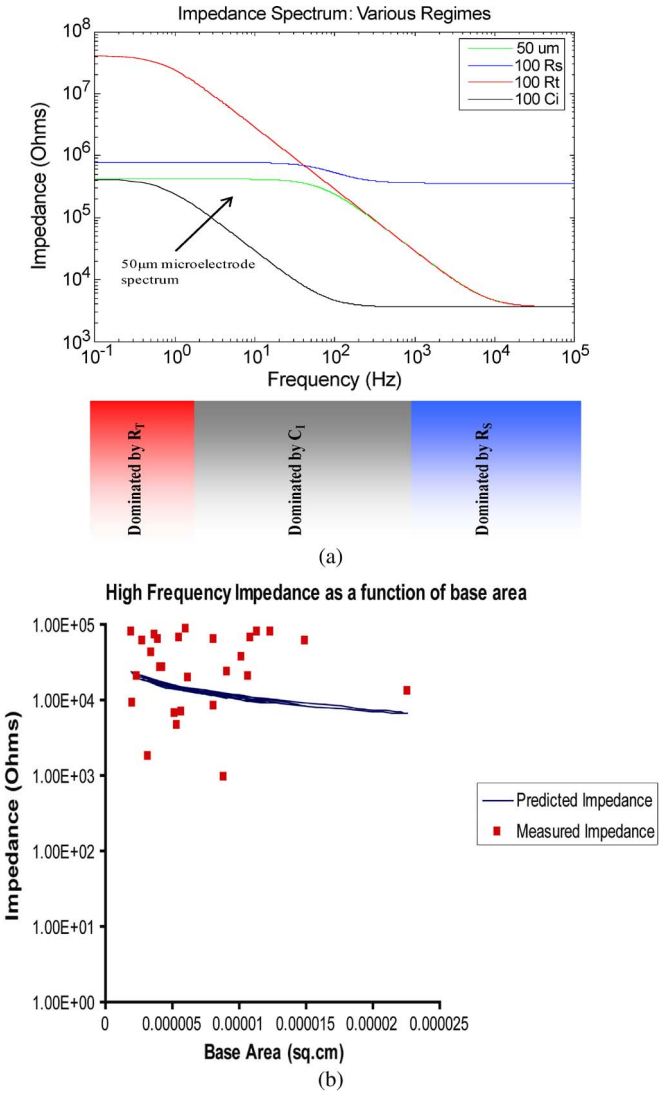


Fig. 10. Electrical impedance modeling versus experimental results: (a) Modeling results for the various regimes of the individual components in the model. (b) Modeling versus experimental results for high-frequency impedance depicting a trend.

TABLE I
COMPARISON BETWEEN MODELING AND EXPERIMENTAL PARAMETERS FOR ELECTRODE IMPEDANCE MODEL

| Parameter | Value (Model) | Value (Experimental) |
|---|---|---|
| $C_I$ | 0.031pF/µm$^2$ | 0.07 pF/µm$^2$ |
| $J_0$ | 1.23 x 10$^{-7}$ A/cm$^2$ | 2 x 10$^{-9}$ A/cm$^2$ |
| ρ | 123 Ω.cm | 72 Ω.cm |

dynamic signal analyzer augmented with a custom-built controlled switching board that allows for rapid automated measurements of the magnitude and phase of microelectrode impedances across a large range of frequencies (1 mHz–100 kHz). Impedance measurements were performed between the microelectrode, ground, and the cellular conducting media (Hank's Balanced Salt Solution, *Invitrogen Corporation*, Carlsbad, CA). The fabricated and packaged 3-D MEAs were interfaced with this custom setup, and each electrode was scanned. Fig. 11(a) shows the impedance spectroscopy measurements of the 3-D MEA (laser micromachining/RIE technique). The same result for the "capped" 3-D MEAs is shown Fig. 11(b), depicting the higher yield of this process compared with that of laser microablation.

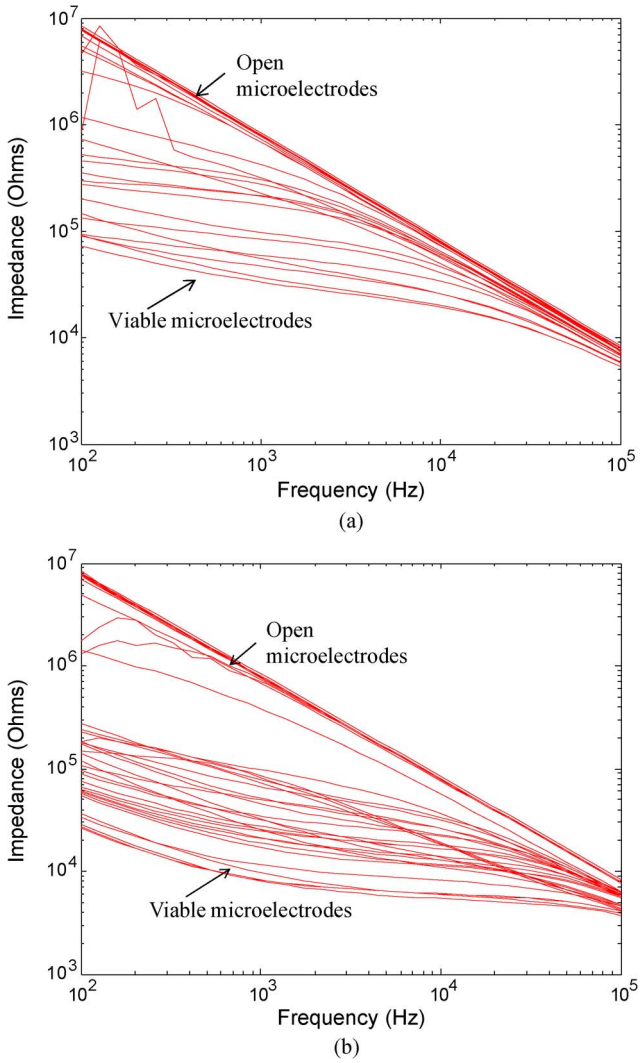


Fig. 11. Electrical impedance spectroscopy results: (a) Representative results for an MTM 3-D MEA with recording sites defined utilizing a laser micromachining/RIE process. (b) Same result for a representative MEA with recording sites defined utilizing a "capping" process showing improved yield.

### *C. Biocompatibility Evaluation With 2-D Planar Cultures of Neurons*

Several new materials like PMMA, PU, and laser-micromachined parylene are being introduced in this paper to microelectrode fabrication by the MTM process. The biocompatibility of these materials needs to be evaluated before these MEAs can be tested for electrophysiological stimulation and recording of dissociated cultures or slices. The evaluation of biocompatibility was carried out as part of this work, utilizing 2-D planar cultures of rat neurons (from the cortex). The procedure for extraction of neurons from pregnant rats is given in detail by Cullen and LaPlaca [36] and was approved by the Georgia Institute of Technology (Georgia Tech)'s Institutional Animal Care and Use Committee (IACUC). The extracted neuronal cells were plated as a planar culture at a cell density

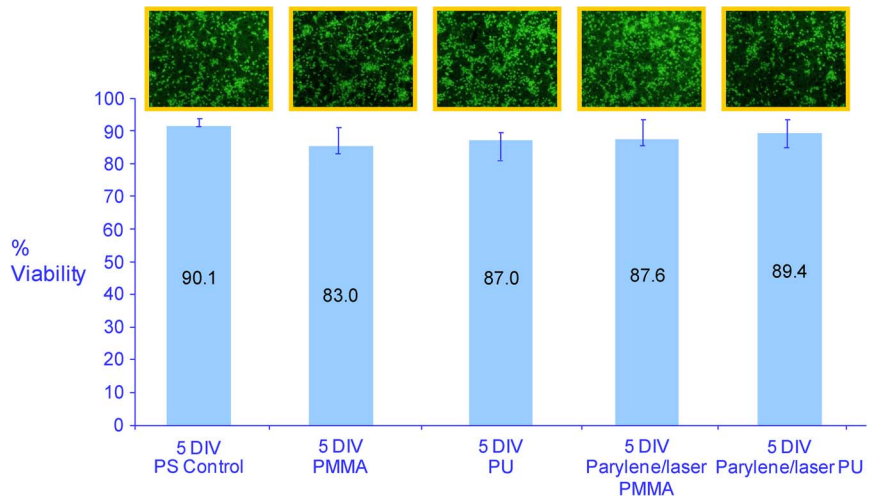


Fig. 12. Fluorescent microscopy images of 2-D planar neuronal cultures growing on various substrates after five DIV and percentage viability of all MTM samples tested with controls.

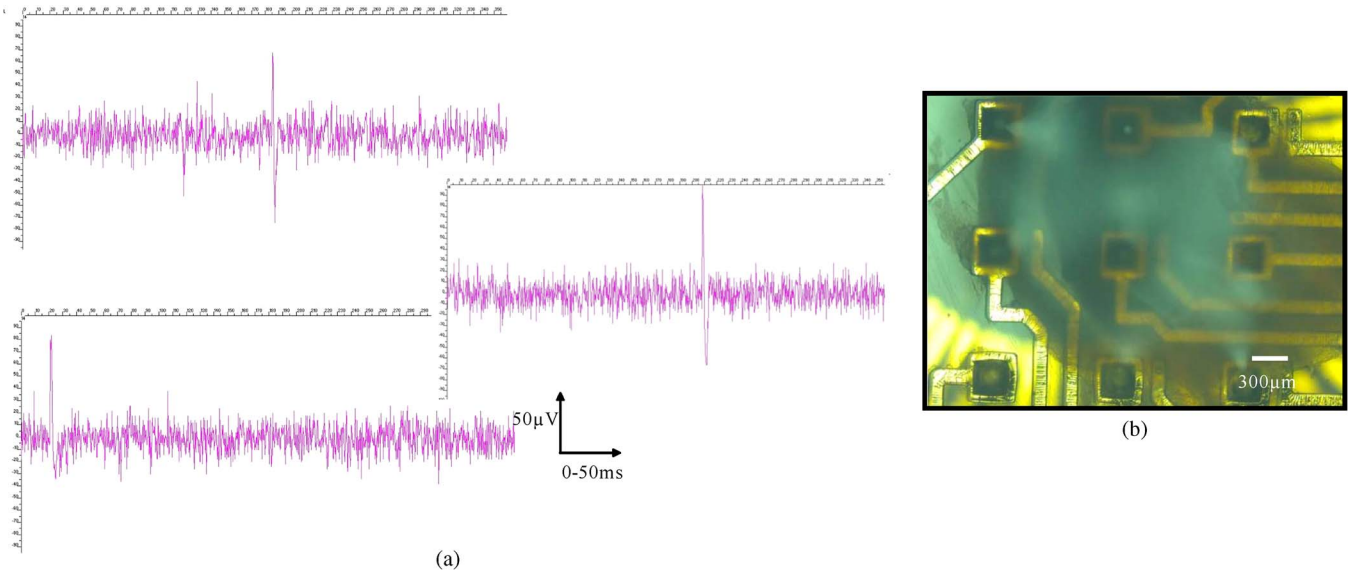


Fig. 13. (a) Electrophysiological spike recordings from brain slices of ten-day postnatal rat pups on three separate electrodes. (b) Optical micrograph of a tissue slice on a 3-D MEA.

of 1250–2500 cells/mm$^2$ on the following samples: 5-mm$^2$ pieces of PMMA, PU, parylene-coated/laser-scribed PMMA, parylene-coated/laser-scribed PU, and a 12-well control plate of polystyrene. The cultures were maintained at 37° C and 5% $CO_2$-95% humidified air in an incubator. The cultures were evaluated daily (by optical microscopic inspection) for survival, and the media was changed every 24 h for five days. Live/dead imaging was performed at five days using confocal microscopy (multiphoton excitation confocal microscope, LSM 510 NLO META, *Carl Zeiss, Inc.*, Oberkochen, Germany). Prior to imaging, the samples were fluorescently stained with 1.6-$\mu$M Hoechst 33 258 and 3-$\mu$M propidium iodide (*Molecular Probes*, Eugene, OR). The details of procedures for live/dead staining are described in [36]. Fig. 12 (top) shows the fluorescent microscopy images for all five samples. The viability was evaluated by counting the number of live cells (fluorescing green) and the number of cells with compromised membranes (nuclei fluorescing red) at five days *in vitro* (DIV). The counting was performed under the confocal microscope by isolating five regions in each culture and averaging the cell count across these regions. Viability is expressed as a percentage of the number of live cells divided by the total number of cells plated. The viability of all the materials was comparable with the 12-well plate, as shown in Fig. 12 (bottom). The value of viability for all the materials was within the range: 85% $\pm$ 5.1%. This demonstrates excellent biocompatibility of the materials involved in the MTM process (with respect to neuronal cells).

### *D. Electrophysiological Spike Recordings From Tissue Slices*

Electrophysiological recordings were performed using hippocampal slices from ten-day postnatal rat pups. The dissection procedures for tissue slices are provided in detail by McClain *et al.* [37] and were approved by the Georgia Tech's IACUC. Briefly, a hippocampal brain tissue was isolated from

postnatal Sprague Dawley rat pups at day 10. The pups were anesthetized with 5% isofurane in oxygen prior to decapitation and harvest, which was performed within 10 min of sacrifice on a chilled surface to maximize tissue viability. The hippocampi were removed from the brain and sectioned into 500-$\mu$m-thick slices using a McIlwain Tissue Chopper (*Mickly Laboratories and Engineering*, Surrey, England). Three slices were separated in Gey's balanced salt solution (*Sigma-Aldrich*, St. Louis, MO) and arranged on the 3-D MEA and held in place by an organotypic cell culture membrane (*Greiner Bio-One*, Monroe, NC) and a stainless steel ring. A room-temperature oxygenated extracellular-based buffered salt solution bathed the slices during the recording session. To enhance neural firing, the potassium concentration was elevated to higher than normal physiological levels at 20 mM. Recording was done on multiple sets of freshly dissected slices using a recording preamplifier (MEA 1 060) and MC Rack software (*MCS*, Reutlingen, Germany). Fig. 13(a) shows individual spikes from three different electrodes that are greater than $\pm 50$ $\mu$V. Fig. 13(b) shows an optical image of a tissue slice on a 3-D MEA. This demonstrates the ability of metal-transfer-molded 3-D MEAs to successfully record electrical spikes from neuronal aggregates. Studies on burst patterns and spike recognition algorithms are outside the scope of this paper.

## V. Discussion and Conclusion

Microelectrode arrays are an important tool in the study of neuronal cultures and brain slices. *In vitro* models of neuronal cultures are becoming more popular in physiology and pharmacology as they show better performance metrics compared with their *in vivo* counterparts. The research standard for MEAs are planar 2-D MEAs but these suffer from rapid data attenuation in the $z$-direction when stimulating/recording from 3-D dissociated cultures like tissue slices. Three-dimensional MEAs are required for these types of cultures. Integrated 3-D MEAs are relatively rare due to the complex nature of the MEMS technologies that are needed to fabricate and package them. We have demonstrated one such technology: MTM, which has the potential to not only fabricate 3-D MEAs relatively easily but also to mass produce them. We have further packaged the MEAs on custom-designed PCBs. We have taken the well-established electrode–electrolyte theory and applied it to our 3-D MEAs. The impedance predicted by the theory and the spectrum obtained through experiments agree in the same degree as other complex MEA approaches. We have also developed a metric to tailor the high-frequency impedance of a 3-D MEA to suit the application. Polymers like PU and PMMA have been introduced to MEA fabrication, and the biocompatibility of these materials has been evaluated using 2-D planar cultures of neurons. These materials show excellent cell viability after five DIV. Finally, electrophysiological passive spike recordings have been performed utilizing brain slices from the hippocampus region of ten-day postnatal rat pups. This technology demonstrates excellent promise for manufacturing-friendly 3-D MEAs and potentially answers the needs of the electrophysiological and pharmacological communities.

## Acknowledgment

The authors would like to thank B. Wester for his assistance with the MEA schematic and 3-D process schematics, Dr. F. Cros, C. Justice, and W. P. Galle for their assistance in packaging the MEAs as well as the valuable technical discussions. The microfabrication portion of this work was performed at the Microelectronics Research Center cleanroom.

## References

[1] S. M. Potter, D. A. Wagenaar, and T. B. DeMarse, "Closing the loop: Stimulation feedback systems for embodied MEA cultures," in *Advances in Network Electrophysiology Using MEAs*, M. Taketani and M. Baudry, Eds. New York: Springer-Verlag, 2006.

[2] S. A. Boppart, B. C. Wheeler, and C. S. Wallace, "A flexible perforated microelectrode array for extended neural recordings," *IEEE Trans. Biomed. Eng.*, vol. 39, no. 1, pp. 37–42, Jan. 1992.

[3] Y. Nam, B. C. Wheeler, and M. O. Heuschkel, "Neural recording and stimulation of dissociated hippocampal cultures using microfabricated three-dimensional tip electrode array," *J. Neurosci. Methods*, vol. 155, no. 2, pp. 296–299, Sep. 2006.

[4] C. A. Thomas, P. A. Springer, G. E. Loeb, Y. Berwald-Netter, and L. M. Okun, "A miniature microelectrode array to monitor the bioelectric activity of cultured cells," *Exp. Cell Res.*, vol. 74, no. 1, pp. 61–66, Sep. 1972.

[5] K. D. Wise and J. B. Angell, "A low-capacitance multielectrode probe for use in extracellular neurophysiology," *IEEE Trans. Biomed. Eng.*, vol. BME-22, no. 3, pp. 212–219, May 1975.

[6] T. Wang, W. Yang, H. Huang, and C. Fu, "A novel fabrication method of flexible micro electrode array for neural recording," in *Proc. IEEE MEMS Conf.*, Kobe, Japan, 2007, pp. 295–300.

[7] S. P. Lacour, C. Tsay, S. Wagner, Z. Yu, and B. Morrison, III, "Stretchable micro-electrode arrays for dynamic neuronal recording of in vitro mechanically injured brain," in *Proc. IEEE Sensors*, 2005, pp. 4–8.

[8] M. O. Heuschkel, M. Fejtl, M. Raggenbass, D. Bertrand, and P. Renaud, "A three-dimensional multi-electrode array for multi-site stimulation and recording in acute brain slices," *J. Neurosci. Methods*, vol. 114, no. 2, pp. 135–148, Mar. 2002.

[9] N. P. Pham, E. Boellaard, J. N. Burghartz, and P. M. Sarro, "Photoresist coating methods for the integration of novel 3-D RF microstructures," *J. Microelectromech. Syst.*, vol. 13, no. 3, pp. 491–499, Jun. 2004.

[10] S. Rajaraman, S. O. Choi, R. H. Shafer, J. D. Ross, J. Vukasinovic, Y. Choi, S. P. DeWeerth, A. Glezer, and M. G. Allen, "Microfabrication technologies for a coupled three-dimensional microelectrode, microfluidic array," *J. Micromech. Microeng.*, vol. 17, no. 1, pp. 163–171, Jan. 2007.

[11] S. Linder, H. Baltes, F. Gneadinger, and E. Doering, "Photolithography in anisotropically etched grooves," in *Proc. IEEE Micro Electro Mech. Syst. Conf.*, 1996, pp. 38–43.

[12] K. D. Wise, "Silicon microsystems for neuroscience and neural prostheses," *IEEE Eng. Med. Biol. Mag.*, vol. 24, no. 5, pp. 22–29, Sep./Oct. 2005.

[13] B. Qing, K. D. Wise, and D. J. Anderson, "A high-yield microassembly structure for three-dimensional microelectrode arrays," *IEEE Trans. Biomed. Eng.*, vol. 47, no. 3, pp. 281–289, Mar. 2000.

[14] L. Rowe, M. Almasri, N. Fogleman, A. B. Frazier, and G. J. Brewer, "An active microscaffold for culturing 3-D neuronal networks," in *Proc. 13th IEEE Int. Conf. Solid-State Sens., Actuators, Microsyst. Dig. Tech. Papers. TRANSDUCERS*, 2007, vol. 1, pp. 948–951.

[15] K. E. Jones, P. K. Campbell, and R. A. Normann, "A glass silicon composite intracortical electrode array," *Ann. Biomed. Eng.*, vol. 20, no. 4, pp. 423–437, Jul. 1992.

[16] T. A. Fofonoff, S. M. Martel, N. G. Hatsopoulos, J. P. Donoghue, and I. W. Hunter, "Microelectrode array fabrication by electrical discharge machining and chemical etching," *IEEE Trans. Biomed. Eng.*, vol. 51, no. 6, pp. 890–895, Jun. 2004.

[17] P. Thiebaud, N. F. de Rooij, M. Koudelka-Hep, and L. Stoppini, "Microelectrode arrays for electrophysiological monitoring of hippocampal organotypic slice cultures," *IEEE Trans. Biomed. Eng.*, vol. 44, no. 11, pp. 1159–1163, Nov. 1997.

[18] S. Metz, M. O. Heuschkel, B. Valencia Avila, R. Holzer, D. Bertrand, and P. Renaud, "Microelectrodes with three-dimensional structures for improved neural interfacing," in *Proc. 23rd Annu. Int. Conf. IEEE EMBS*, 2001, pp. 765–768.

[19] K. Takei, T. Kawashima, T. Kawano, H. Takao, K. Sawada, and M. Ishida, "Integration of out-of-plane silicon dioxide microtubes, silicon

microprobes and on-chip NMOSFETs by selective vapor-liquid-solid growth," *J. Micromech. Microeng.*, vol. 18, no. 3, pp. 1–10, Mar. 2008.
[20] H. Lorenz, M. Despont, N. Fahrni, N. LaBianca, P. Renaud, and P. Vettiger, "SU-8: A low-cost negative resist for MEMS," *J. Micromech. Microeng.*, vol. 7, no. 3, pp. 121–124, Sep. 1997.
[21] F. Cros and M. G. Allen, "High aspect ratio structures achieved by sacrificial conformal coating," in *Proc. Solid State Sens. Actuators Workshop*, 2000, pp. 261–264.
[22] Y. K. Yoon, J. H. Park, and M. G. Allen, "Multidirectional UV lithography for complex 3-D MEMS structures," *J. Microelectromech. Syst.*, vol. 15, no. 5, pp. 1121–1130, Oct. 2006.
[23] Y. Zhao, Y.-K. Yoon, S.-O. Choi, X. Wu, Z. Liu, and M. G. Allen, "Three dimensional metal pattern transfer for replica molded microstructures," *Appl. Phys. Lett.*, vol. 94, no. 2, pp. 023 301-1–023 301-3, Jan. 2009.
[24] S. H. Ko, I. Park, H. Pan, C. P. Grigoropoulos, A. P. Pisano, C. K. Luscombe, and J. M. J. Frechet, "Direct nanoimprinting of metal nanoparticles for nanoscale electronics fabrication," *Nano Lett.*, vol. 7, no. 7, pp. 1869–1877, Jul. 2007.
[25] S.-H. Hur, D.-Y. Khang, C. Kocabas, and J. A. Rogers, "Nanotransfer printing by use of noncovalent surface forces: Applications to thin-film transistors that use single-walled carbon nanotube networks and semiconducting polymers," *Appl. Phys. Lett.*, vol. 85, no. 23, pp. 5730–5732, Dec. 2004.
[26] Dow Corning, Inc. [Online]. Available: http://www.dowcorning.com
[27] Du Pont Inc. [Online]. Available: http://www.dupont.com
[28] R. R. Tummala, *Fundamentals of Microsystems Packaging*. New York: McGraw-Hill, 2001.
[29] Ayanda Biosystems. [Online]. Available: http://www.ayanda-biosys.com
[30] Speciality Coating Systems. [Online]. Available: http://www.scscoatings.com
[31] R. L. Pozzo, A. S. Malicsi, and I. Iwasaki, "Removal of lead from printed-circuit board scrap by an electrodissolution delamination method," *Resour. Conserv. Recycl.*, vol. 5, no. 1, pp. 21–34, Feb. 1991.
[32] F. Herrault, C. H. Ji, S. Rajaraman, R. H. Shafer, and M. G. Allen, "Electrodeposited metal structures in high aspect ratio cavities using vapor deposited polymer molds and laser micromachining," in *Proc. IEEE Int. Conf. Solid-State Sens., Actuators, Microsyst. TRANSDUCERS*, 2007, pp. 513–516.
[33] D. A. Borkholder, "Cell based biosensors using microelectrodes," Ph.D. dissertation, Dept. Elect. Eng., Stanford Univ., Palo Alto, CA, 1998.
[34] J. D. Ross, "Microstimulation and multicellular analysis: A neural interfacing system for spatiotemporal stimulation," Ph.D. dissertation, Dept. Bioeng., Georgia Inst. Technol., Atlanta, GA, 2008.
[35] W. Franks, I. Schenker, P. Schmutz, and A. Hierlemann, "Impedance characterization and modeling of electrodes for biomedical applications," *IEEE Trans. Biomed. Eng.*, vol. 52, no. 7, pp. 1295–1302, Jul. 2005.
[36] D. K. Cullen and M. C. LaPlaca, "Neuronal response to high rate shear deformation depends on heterogeneity of the local strain field," *J. Neurotrauma*, vol. 23, no. 9, pp. 1304–1319, Sep. 2006.
[37] M. A. McClain, M. C. LaPlaca, and A. B. Frazier, "A microperfusion system for improved viability in thick slice preparations of brain tissue," in *Proc. 9th Int. Conf. Miniaturized Syst. Chem. Life Sci. (MicroTAS)*, Boston, MA, 2005, pp. 897–899.

**Swaminathan Rajaraman** received the B.S. degree in electronics engineering from Bharathidasan University, Trichy, India, in 1998, the M.S. degree in electrical engineering from the University of Cincinnati, Cincinnati, OH, in 2001, and the Ph.D. degree in electrical engineering from the Georgia Institute of Technology, Atlanta, in 2009.

From 2001 to 2002, he was with the Micromachined Products Division, Analog Devices, Cambridge, MA, where he developed optical MEMS micromirrors for telecommunication applications. From 2004 to 2005, he was with CardioMEMS, Atlanta, GA, where he developed implantable MEMS pressure sensors for detection of heart diseases. Since 2007, he has been with Axion BioSystems, Inc., Atlanta, where he currently holds the title of Director of MEMS R&D/Manufacturing. His current research interests include NeuralMEMS, micro-/nanofabrication, microneedles, microtweezers, micro-total analysis systems, nanosensors, and implantable MEMS devices.

Dr. Rajaraman was the Track Chair for the Bioelectric Sensors session at the IEEE Engineering in Medicine and Biology Conference 2010.

**Seong-O Choi** received the B.S. degree in physics from Yonsei University, Seoul, Korea, in 1998, the M.S. degree in biomedical engineering from the University of Southern California, Los Angeles, in 2001, and the M.S. and Ph.D. degrees in electrical and computer engineering from the Georgia Institute of Technology, Atlanta, in 2003 and 2007, respectively. During his Ph.D. studies, his research focused on the development of electrically active 3-D microstructures utilizing inclined UV lithography and metal transfer micromolding for biomedical applications including microneedle arrays for electroporation and 3-D microelectrode arrays for neural recording/stimulation.

Since 2008, he has been with the School of Chemical and Biomolecular Engineering, Georgia Institute of Technology, as a Postdoctoral Fellow. His current research interests include vaccination using microneedles, implantable microdevices for controlled drug delivery, and 3-D fabrication technology for polymer-based biomedical microsystems.

**Maxine A. McClain** (M'10) received the B.S. degree in biomedical engineering and the M.S. degree in electrical engineering from The Catholic University of America, Washington, DC, in 1998 and 2000, respectively, and the Ph.D. degree in electrical engineering in the area of biomicroelectromechanical systems and neuroelectrode technologies from the Georgia Institute of Technology, Atlanta, in 2010.

She was a Postgraduate Researcher at Oak Ridge National Laboratory, Oak Ridge, TN, developing lab-on-a-chip assays for cellular analysis. She is currently with Axion Biosystems, Inc., Atlanta.

**James D. Ross** (S'04) received the B.S. degree in electrical engineering, with an emphasis on semiconductors, from Louisiana State University, Baton Rouge, in 2000, and the Ph.D. degree in biological engineering from the Georgia Institute of Technology, Atlanta, in 2008.

Since 2008, he has served as the Chief Technology Officer of Axion Biosystems, Inc., Atlanta, where he applies microelectrode array technology to applications in life-science instrumentation and medical devices.

**Michelle C. LaPlaca** received the B.S. degree in biomedical engineering from The Catholic University of America, Washington, DC, in 1991, and the M.S.E. and Ph.D. degrees in bioengineering from the University of Pennsylvania, Philadelphia, in 1992 and 1996, respectively.

Following her postdoctoral training in neurosurgery at the University of Pennsylvania from 1996 to 1998, she has been with the faculty of the Georgia Institute of Technology (Georgia Tech), Atlanta. She is currently an Associate Professor in The Wallace H. Coulter Department of Biomedical Engineering, a joint department between Georgia Tech and Emory University. Her current research interests are in traumatic brain and spinal-cord injuries, neural tissue engineering, injury biomechanics, neural interfacing, and cognitive impairment associated with brain injury and aging.

Dr. LaPlaca is a member of the National Neurotrauma Society, Women in Neurotrauma Research, the Society for Neuroscience, the American Society for Neural Therapy and Repair, The American Physiological Society, and the Biomedical Engineering Society.

**Mark G. Allen** (F'10) received the B.A. degree in chemistry, the B.S.E. degree in chemical engineering, and the B.S.E. degree in electrical engineering from the University of Pennsylvania, Philadelphia, and the S.M. and Ph.D. degrees from the Massachusetts Institute of Technology (MIT), Cambridge, in 1989.

In 1989, he joined the faculty of the School of Electrical and Computer Engineering, Georgia Institute of Technology (Georgia Tech), Atlanta, where he currently holds the rank of Regents' Professor and the J.M. Pettit Professorship in Microelectronics. He also held the position of Senior Vice Provost for Research and Innovation at Georgia Tech from 2007 to 2010 and, in that capacity, was charged with overseeing Georgia Tech's interdisciplinary research centers, managing Georgia Tech's sponsored research portfolio, and guiding the commercialization of Georgia Tech research results and intellectual property. He is currently the Editor-in-Chief of the *Journal of Micromechanics and Microengineering*. His current research interests are in the field of micro- and nanofabrication technology, with emphasis on new approaches to fabricate devices with characteristic lengths in the micro- to nanoscale from both silicon and nonsilicon materials.

Dr. Allen was the Cochair of the 1996 IEEE/ASME Microelectromechanical Systems Conference and is the Regional Cochair (Americas region) for the IEEE Transducers Conference in 2011. He is a member of the MIT Corporation Visiting Committee for Sponsored Research.